# 14TH INTERNATIONAL CONFERENCE ON HYDROSCIENCE AND ENGINEERING


**PROCEEDINGS BOOK**

EDITORS

Prof. Dr. Şebnem ELÇİ

Assoc. Prof. Dr. Gökçen BOMBAR

14TH INTERNATIONAL CONFERENCE
ON HYDROSCIENCE & ENGINEERING
MAY 26-27, 2022
IZMİR-TURKEY

# IMPROVING WRF-HYDRO EXTREME RUNOFF SIMULATIONS THROUGH THE SEA SURFACE TEMPERATURE FIELDS WITH HIGHER SPATIO-TEMPORAL RESOLUTION

*First Author: Berina M. Kilicarslan*

Civil Engineering Department, Middle East Technical University

Ankara, Turkey

berinakilicarslan@gmail.com

*Ismail Yucel*

Civil Engineering Department, Middle East Technical University

Ankara, Turkey

iyucel@metu.edu.tr

*Tugrul Yilmaz*

Civil Engineering Department, Middle East Technical University

Ankara, Turkey

tuyilmaz@metu.edu.tr

ABSTRACT: This study investigates the impact of the spatio-temporal accuracy of four different sea surface temperature (SST) datasets on the accuracy of the Weather Research and Forecasting (WRF)-Hydro system to simulate hydrological response during two catastrophic flood events over the Eastern Black Sea (EBS) and the Mediterranean (MED) regions of Turkey. Three daily-updated and high spatial resolution external SST products (GHRSST, Medspiration, and NCEP-SST) and one coarse-resolution and time-invariant SST product (ERA5- and GFS-SST for EBS and MED regions, respectively) already embedded in the initial and the boundary conditions datasets of WRF model are used in deriving near-surface atmospheric variables through WRF. Event-based calibration is performed to the WRF-Hydro system using hourly and daily streamflow data in both regions. The uncoupled model simulations for independent SST events are conducted to assess the impact of SST-triggered precipitation on simulated extreme runoff. Some localized and temporal differences in the occurrence of the flood events with respect to observations depending on the SST representation are noticeable. SST products represented with higher cross-correlations (GHRSST and Medspiration) revealed significant improvement in flood hydrographs for both regions. The GHRSST dataset shows a substantial improvement in NSE (~70%) and KGE (from 0.06 to 0.3) with respect to the invariable SST (ERA5) in simulated runoffs over the EBS region. Reduction in RMSE up to 20% and an increase in correlation from 0.3 to 0.8 is observed for the same region. The use of both GHRSST and Medspiration SST data characterized with high spatio-temporal correlation resulted in runoff simulations exactly matching the observed runoff peak of 300 m3/s by reducing the overestimation seen in invariable SST (GFS) in the MED region.

## 1. INTRODUCTION

Extreme weather events result in devastating flood catastrophes with casualties in today's world. As the climate warms, more water vapor is pumped into the atmosphere, increasing the severity of rainfall events. With the changing climate, the impact of flood disasters may be worsened over time (Allen & Ingram, 2002).

As a result, reliable flood forecasting is critical for various operational purposes. One of the most crucial components of an accurate flood forecasting system is accurate estimates of the spatial distribution and the intensity of heavy rainfall events and their associated hydrologic responses (Yucel & Onen, 2014). Flood forecasting applications based on a hydro-meteorological modeling framework

that integrates the atmosphere-hydrology are becoming more prevalent in this regard (Kunstmann & Stadler, 2005). More accurate flood forecasts essentially necessitate enhanced Numerical Weather Prediction (NWP) forecasts. Thus, the accuracy of short-term predictions is strongly influenced by the choice of the NWP model and the inputs that drive the initial & boundary conditions (Done et al., 2004).

The ocean/sea-atmosphere interaction is the starting point that determines the climate distribution of the entire Earth. With this interaction, every change in the atmosphere determines the regional climate types and the distribution of these climates on the planet by moving vertically and horizontally with the effect of the Earth's daily and annual movement, ocean currents, winds, and topography (Bigg et al., 2003). SST is one of the most influential variables in this mentioned ocean-atmosphere interaction. Studies conducted particularly over the coastline with steeply varying topography address the fact that an accurate parameterization of the linkage between the land and atmosphere systems is required to demonstrate changes in water and energy fluxes and states for a more realistic flood prediction. To improve the reliability of such modeling systems, it is necessary to consider factors affecting this linkage. Therefore, the SST representation in the modeling system is regarded as one of the factors having a pronounced effect on water and energy fluxes in the lower-level atmosphere. Therefore, the condition of the SST has a substantial impact on the state of meteorological forcing variables in such NWP models, as the sea acts as a water and energy source for both the atmosphere and the land surface (Lebeaupin et al., 2006). Accordingly, providing high accuracy SST input to the lower boundary is crucial for accurate precipitation modelling, hencefor better flood forecasts through hydrological models.

The WRF-Hydro is a distributed, multi-physics hydrometeorological model system created by the United States National Center for Atmospheric Research (NCAR) to address major water challenges, including operational flash flood monitoring. Many studies have utilized this modeling system to examine the model's performance and applicability, including flood predictions, water balance, and water management studies across the globe (Kerandi et al., 2018; Li et al., 2017). Despite the studies compare the impact of different sources of precipitation input (i.e., comparing observed and simulated) on runoff simulation and agree that further improvement in the precipitation simulation skills is still needed (Givati et al., 2016; Senatoreet al., 2015), not many studies have investigated the impact of the spatio-temporal resolution of various SST sources over the runoff predictions of WRF-Hydro modelling system via the improvements in the simulated precipitation. In this study, to expand on the argument, different SST products are utilized in the WRF/WRF-Hydro modeling frameworks to see the impact of the temporal and spatial resolution-wise improved representation of the SST on the simulations of extreme precipitation causing significant floods over the catchments of regions in Turkey. In this context, basins and events from different geographic regions as EBS and MED represented with humid and semi-arid climates, respectively are chosen to see the SST impact on the hydrological response.

## 2. DATA AND METHOD

### 2.1. Study Area and Events

Flood events caused by heavy rainfall events that took place in the EBS and MED regions, which have different climatic characteristics are simulated. Figure 1 depicts 3-km domains (d02) the of WRF model encompassing both regions, as well as chosen basins and the associated channel networks and the locations of rain and stream gauge stations.

In this study, two significant flood events occurred in the past are selected for the following modeling practices. On August 24th, 2015, it was reported 32.4 millimeters of hourly precipitation, a total of 135 mm of rain fell during 24 hours over Artvin-Arhavi province in the EBS region. As an alternative event, on December 16th, 2018, the Antalya-Ovacik station reported an hourly precipitation of 53.1 mm, while receiving a total of 651.7 millimeters on the same day. This was the heaviest rainstorm ever recorded over the entire Turkey (Kaya et al., 2019). This recorded value was around three times greater than the Antalya city's monthly average rainfall in December (265.3 mm). A typical mesoscale

convective signal was observed for the event that occurred over the EBS area in the summer, whereas a frontal system was dominating for the event that occurred over the MED region in the winter.

For the evaluation of the model performance, streamflow data from the Arhavi provincial stations D22A049, D22A079, D22A089, and D22A147 (Hopa province), as well as the MED stations D08A071, D09A095, and E08A008 (Figure 1 and Table 1). Each calibration event in Table 1 is run for 10 days to allow the model to warm up. Average streamflow observations (m3/s) collected by the State Hydraulic Works (SHW) of Turkey are provided at daily timesteps at five of the stream gauge stations (D22A079, D22A089, and D22A147 over EBS region; D09A095 and E08A008 over MED region) and hourly timesteps at two of the stations (D22A049 over EBS and D08A071 over MED). However, the hourly streamflow data at these two stations are limited and only available after 2016.

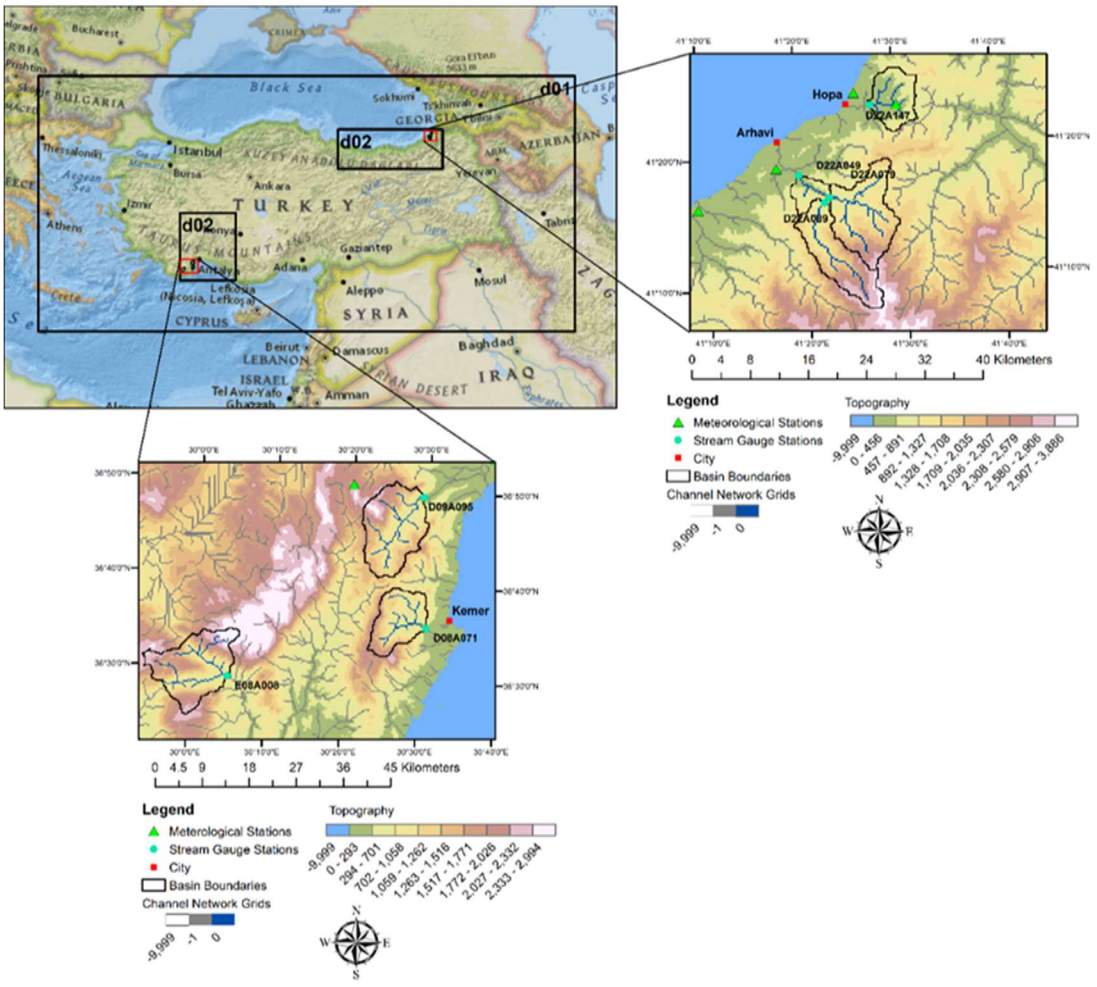


Figure 1 The outer and nested domains (d01 and d02) of the WRF model for the EBS and MED regions are displayed in the top-left. The boundaries of the selected basin, their outlet points (stream gauge stations denoted as blue dots), channel network grids in the WRF-Hydro model, and the meteorological station (denoted as a green triangle) are shown in the zoomed maps with the high-resolution topography layer in the background for the EBS region (top-right) and the MED region (bottom).

Table 1. Drainage areas and calibrated event periods of each selected basin over EBS and MED regions.

| Region | Station | Drainage Area ($km^2$) | Calibration Event Period | |
|---|---|---|---|---|
| | | | Start | End |
| EBS | D22A049 | 175.8 | 08/27/2016 | 09/06/2016 |

| | | | | |
|---|---|---|---|---|
| | | | 09/20/2017 | 09/30/2017 |
| | | | 10/19/2016 | 10/29/2016 |
| | D22A079 | 85.8 | 10/19/2016 | 10/29/2016 |
| | | | 10/01/2018 | 01/11/2018 |
| | | | 06/24/2019 | 07/04/2019 |
| | D22A089 | 71.5 | 08/27/2016 | 09/06/2016 |
| | | | 09/20/2017 | 09/30/2017 |
| | | | 10/19/2016 | 10/29/2016 |
| | D22A147 | 41.9 | 08/27/2016 | 09/06/2016 |
| | | | 09/20/2017 | 09/30/2017 |
| | | | 10/19/2016 | 10/29/2016 |
| | D08A071 | 98.3 | 01/09/2015 | 01/19/2015 |
| | | | 03/07/2017 | 03/17/2017 |
| | | | 03/23/2015 | 04/02/2015 |
| MED | E08A008 | 164.5 | 01/09/2015 | 01/19/2015 |
| | | | 03/07/2017 | 03/17/2017 |
| | | | 03/23/2015 | 04/02/2015 |
| | D09A095 | 164.6 | 01/21/2014 | 01/31/2014 |
| | | | 01/09/2015 | 01/19/2015 |
| | | | 03/23/2015 | 04/02/2015 |

2.2. Sea Surface Temperature Field Update in WRF Model

Along with the time-invariant SSTs (ERA5 and GFS), three additional daily-updated SST datasets are employed in this sensitivity analysis: 1) Medspiration Ultra-High-Resolution Foundation Sea Surface Temperature (CERSAT, 2012); 2) The Group for High-Resolution Sea Surface Temperature Level 4 Ultra-High Resolution (GHRSST) (Team GHRSST, 2010a, 2010b); 3) Real-Time, Global, Sea Surface Temperature (RTG_SST_HR) represented by the National Centers for Environmental Prediction (NCEP), National Oceanic and Atmospheric Administration (NOAA) (NCEP & NOAA, 2014). Medspiration, GHRSST, and NCEP SST datasets are available in daily time step and have high spatial resolutions of 0.022°, 0.01°, and 0.083°, respectively. Medspiration, GHRSST, NCEP, ERA5, and GFS will be used to refer to the simulations performed with different SST products utilized in this work henceforth. Table 2 depicts the simulation dates for the WRF model utilizing these SST products for each area of study.

Table 2. Forcings used in the SST simulations and their run periods.

| Region | Forcings | | Run Periods | |
|---|---|---|---|---|
| | SST Products | Initial and Boundary Conditions | Start | End |
| EBS | ERA5<br>GHR<br>Medspiration<br>NCEP | ERA5 Reanalysis | 08/17/2015 | 08/27/2015 |
| MED | GFS<br>GHR<br>Medspiration<br>NCEP | GFS Forecast | 12/10/2018 | 12/20/2018 |

### 2.3. WRF-Hydro Model

The integrated hydrological model system named WRF-Hydro (version 5.1.1) is operated in this study (Gochis et al., 2020). The WRF-Hydro hydrological modeling system is an enhanced version of the traditional 1-dimensional Noah-MP LSM that incorporates overland, saturated subsurface, channel, and groundwater flow into a modeling structure. The LSM in the WRF-Hydro model is the same as the one-dimensional LSM (Noah-MP) operated in the WRF model. Accordingly, the hydrological modeling system is operated over the nested domain of WRF (d02) with a 3 km resolution. There are two options available in the modeling system configuration for the feedback mechanisms between WRF and WRF-Hydro model as uncoupled and coupled modes. In uncoupled mode, there is only one-way feedback from atmosphere to land. The meteorological inputs for this mode can be created by WRF model or other sourced such as radar and satellite precipitation can be used.

WRF-Hydro model disaggregates the LSM grids into high-resolution routing grids after the moisture states are computed for the land surface column. In this study LSM grid resolution is defined as 3 km (same as the WRF) and disaggregated into routing grids with a 250 m grid size in both regions.

### 2.4. Calibration of the WRF-Hydro Model

WRF-Hydro calibration runs are performed with the WRF meteorological forcings updated with the observed precipitation. Calibration of the WRF-Hydro is carried out for three events in each basin (seven basins, Table 1) at hourly or daily time steps depending on the availability of streamflow data. The validation of the calibrated parameters sets is performed with the SST simulations. In the D22A049 basin of the EBS region and D08A071 basin of the MED region, hourly streamflow data for two heavy precipitation events in the 2016 and 2017 hydrologic years are used to calibrate the model while other events are calibrated on a daily basis (Table 1). For the validation process (with SST events), hourly streamflow data is only available for the MED region, whereas the daily streamflow is used for the EBS region. The calibrated parameter set of the WRF-Hydro model is then validated for SST simulations over both regions. WRF-Hydro model is forced by meteorological forcings constructed using the ERA5 and GFS SSTs, as well as three additional daily-updated SST

datasets namely Medspiration, GHRSST, and NCEP. Additionally, similar SST events are modeled by substituting observed precipitation in WRF precipitation. The model is calibrated manually using a step-wise approach allowing the model to first simulate the water balance in the basin and then distribute the amount of water accurately over time ((Yucel et al., 2015)). At each step, a common parameter value was determined for all three events, and the calibration of the next parameter was started. This was done based on the visual scanning of hydrographs and the calculated statistics.

## 3. RESULTS

### 3.1. Evaluation of Precipitation Simulations for SST Events

Time series of the basin averaged simulated and observed precipitation for the SST events over D22A147 and D08A071 basins are given in Figure 2 (a) and (b), respectively. Figure 2 (a) shows the precipitation time series from 08/17/2015 00:00:00 UTC to 08/27/2015 00:00:00 UTC, for 241-hours. The highest precipitation at D22A147 is recorded at the 178th hour, or 08/24/2015 09:00:00 UTC as 26.3 mm of rain. However, the highest precipitation quantity over the whole EBS region is reported as 32.4 millimeters at 08/24/2015 00:00:00 UTC within the boundary of D22A049. In spite of this, as shown in Figure 2 (a), the D22A147 basin-average precipitation is calculated as 16.1 mm during the 169th hour, which coincides with the event peak timing over the EBS region. Although simulations with alternative SST datasets are able to approximate the broad pattern, except the primary peak is generated a few hours sooner than observed. In addition, it is seen that the GHRSST simulation underestimates the recorded peak precipitation. A substantial overestimation of the peak value for the GHRSST simulation corresponds to the observed peak, while the other simulations recreate peak values to the observed one.

The time series of the basin-averaged precipitation for the event between 12/10/2018 00:00:00 UTC-12/20/2018 00:00:00 UTC (241-hours) are shown in Figure 2 (b). Peak precipitation is recorded as 53.1 mm during the 162nd hour, corresponding to 12/10/2018 at 17:00:00 UTC. At the same time step, the peak basin-average precipitation for D08A071 is recorded as 15.7 mm. On the whole, all simulated precipitations reveal an almost exact match to the observed patterns, with modest overestimations. On the other hand, high-resolution SST simulations seem to be able to enhance the volume with decreased bias in line with the observation. Simulations performed with GFS SST, GHRSST, and NCEP SST all have slight delays in their peak timing (about 1-2 hours).

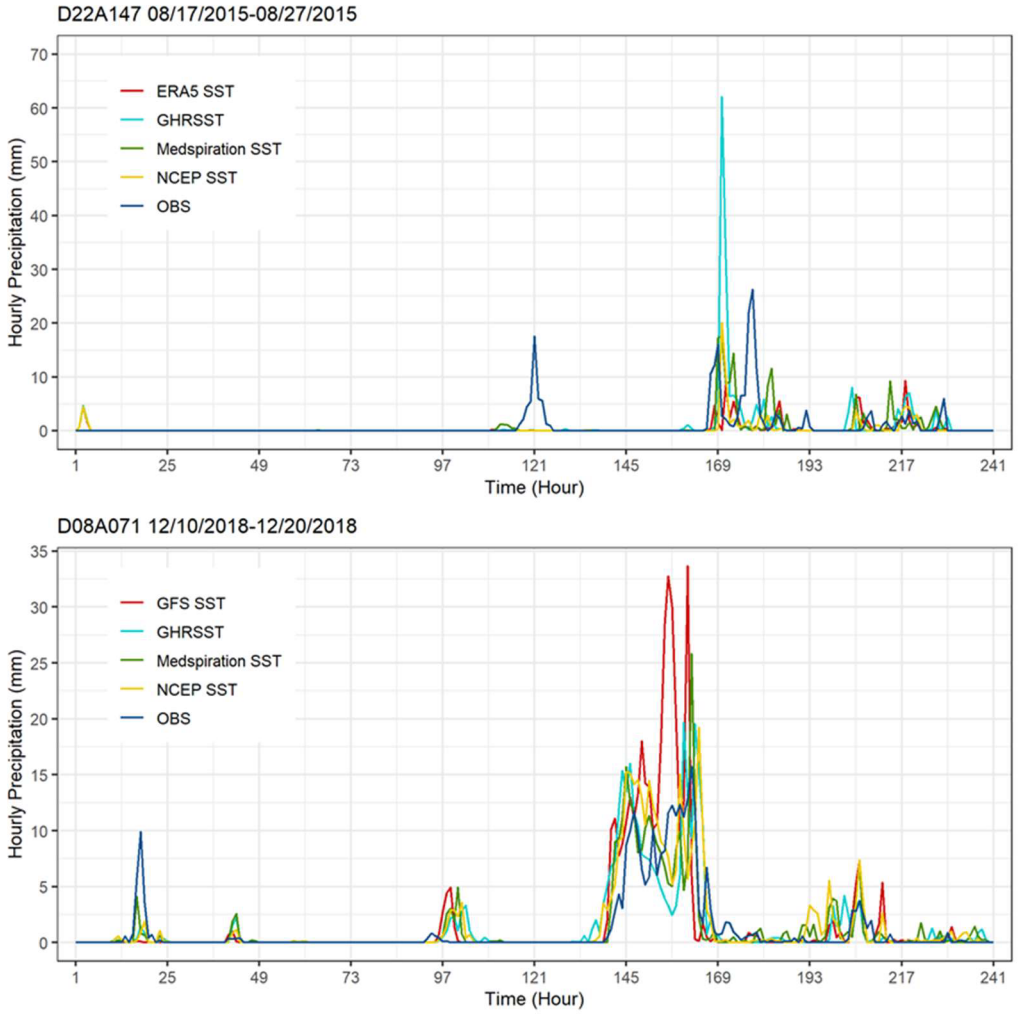


Figure 2. Time series of hourly precipitation that a) D22A147 basin over EBS region receives during the event occurred in 08/17/2015-08/27/2015 and b) D08A071 basin over MED region receives during the event occurred in 12/10/2018-12/20/2018 for ten days. Outputs are generated from the WRF model with the native SST field from ERA5 Reanalysis data (ERA5-SST) for the EBS region and GFS Forecast data (GFS-SST) for the MED region different SST products: GHRSST, Medspiration, and NCEP

### 3.2. Evaluation of SST Events for WRF-Hydro Model

WRF-Hydro model performances of the simulations forced by the WRF meteorological data generated with different SST datasets are examined in this section. The calibrated parameter set with the manual stepwise calibration method is utilized for Hopa (D22A147) and Kemer (D08A071) basins. The simulated hydrograph based on the observation precipitation forcing is also compared with the hydrographs forced by the WRF model to be able to see the errors caused by the interpolation process and the model itself.

Hydrological response to selected SST events over Hopa and Kemer basins is simulated, and the hydrographs derived by various SST simulations and observed precipitation are demonstrated in Figure 3. Based on the simulated hydrograph of the Hopa basin, it is observed that the ERA5 and NCEP simulations are underestimated compared to the observed hydrograph (Figure 3 (a)). The negative bias found for the WRF precipitation simulations in Figure 3 (a) may explain this underestimation issue for ERA5 and NCEP (datasets showing the highest bias error). The hydrograph volumes produced by the Medspiration simulation and the simulation using observed precipitation are marginally better than those produced by the ERA5 and NCEP simulations. Despite the fact that the GHRSST simulation overestimates precipitation and skips the peak time for Hopa, the daily mean discharge of the GHRSST is the most accurate simulation in predicting discharges. In line with the

results of cross-correlation calculations, it is determined that GHRSST is the best SST product that represents the Arhavi basin and the corresponding event.

In the Kemer basin, it is seen that the GFS simulation overestimated the peak value and missed the timing trend of the observation hydrograph (812.9 m3/s) (Figure 3 (b)). The simulations derived using high-resolution SST and observation precipitation shows that although the hydrographs follow a similar trend with the observation in the falling limb part, they decrease abruptly in the rising limb part. Minor delays are observed in the primary peak time for the high-resolution SST simulations. In particular, the simulation forced with the observed precipitation correctly identifies the time and magnitude of the first peak but produces a negative bias in the value of the second peak. High-resolution SST simulations improve the ERA5 results by ~550 m3/s volume reduction and successfully capture the peak timing.

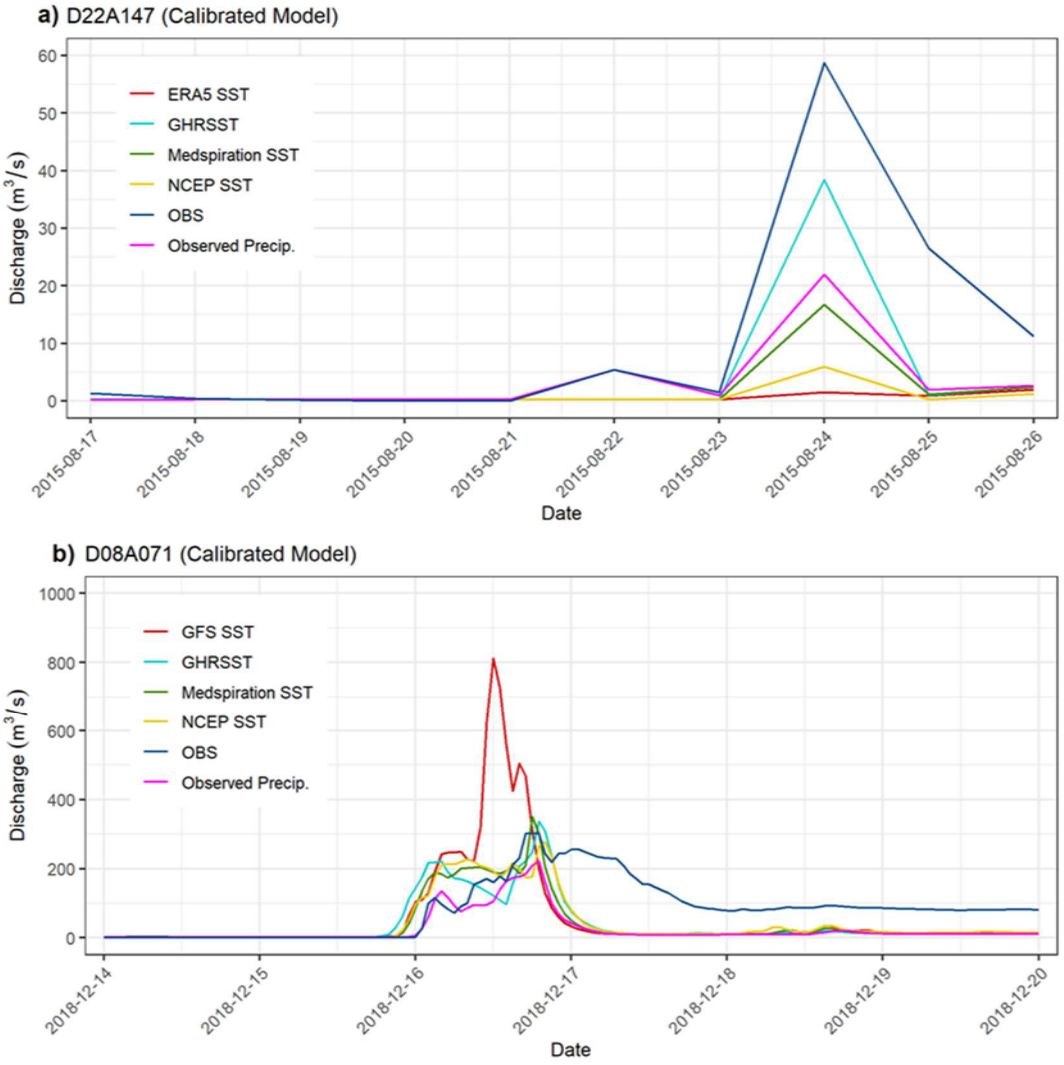


Figure 3 a) 17/08/2015-27/08/2015 event and D22A049 basin b) 03/07/2017-03/17/2017 (last six days) event and D08A071 basin observation hydrograph, modeled hydrographs with the precipitation data generated using ERA5/GFS GHRSST, Medspiration, NCEP SST products, and the modeled hydrograph with the precipitation data based on the interpolation of the observation points

## 4. CONCLUSIONS

Investigation of hydrologic response for extreme precipitation events simulated by different SST datasets integrated into the WRF model with coarse, high, and time-variant and -invariant resolutions in small catchments with a complex topography and experiencing coastal orography was carried out in this study. According to the results of precipitation and hydrograph simulations, high-resolution

SST products may be used as initial and lower boundary conditions for operational forecast purposes for heavy precipitation events. Extreme weather event analyses over coastal regions with complex topography must take atypical SST fluctuations caused by climate change into account using temporally and spatially changing SST characteristics defined by high-resolution datasets. Further improvement of the interflow representation in WRF-Hydro modeling structure may enhance the streamflow simulations and the hydrograph results, particularly at the falling limb stage.

REFERENCES


Allen, M. R., & Ingram, W. J. (2002). Constraints on future changes in climate and the hydrologic cycle. *Nature.Com,* 419(September), 225–232. https://www.nature.com/articles/nature01092 .

Bigg, G. R., Jickells, T. D., Liss, P. S., & Osborn, T. J. (2003). The role of the oceans in climate. *International Journal of Climatology*, *23*(10), 1127–1159. https://doi.org/10.1002/joc.926.

Done, J., Davis, C. A., & Weisman, M. (2004). The next generation of NWP: Explicit forecasts of convection using the weather research and forecasting (WRF) model. *Atmospheric Science Letters*, 5(6), 110–117. https://doi.org/10.1002/asl.72.

Givati, A., Gochis, D., Rummler, T., & Kunstmann, H. (2016). Comparing One-Way and Two-Way Coupled Hydrometeorological Forecasting Systems for Flood Forecasting in the Mediterranean Region. *Hydrology*, *3*(2), 19.

Gochis, D. J., Barlage, M., Cabell, R., Casali, M., Dugger, A., FitzGerald, K., McAllister, M., McCreight, J., RafieeiNasab, A., Read, L., Sampson, K., Yates, D., & Zhang, Y. (2020). The WRF-Hydro modeling system technical description, (Version 5.1.1). *NCAR Technical Note*, 107.

Kaya, O. F., Guler, M., Altan, A., & Yorganci, I. (2019). 15-16-17 Aralık 2018 Tarihlerinde Antalya İli Kemer/Ovacık Mevkiinde Görülen Aşırı Yağış Hadisesinin Aktüel Hava Haritaları, Uzaktan Algılama ve Sayısal Hava Tahmin Ürünleri ile Sinoptik ve Hidrolojik Analizi. *10. Ulusal Hidroloji Kongresi 9-12*, *November*.

Kerandi, N., Arnault, J., Laux, P., Wagner, S., Kitheka, J., & Kunstmann, H. (2018). Joint atmospheric-terrestrial water balances for East Africa: a WRF-Hydro case study for the upper Tana River basin. *Theoretical and Applied Climatology*, *131*(3–4), 1337–1355. https://doi.org/10.1007/s00704-017-2050-8.

Kunstmann, H., & Stadler, C. (2005). High resolution distributed atmospheric-hydrological modelling for Alpine catchments. Journal of Hydrology, 314(1–4), 105–124. https://doi.org/10.1016/j.jhydrol.2005.03.033.

Lebeaupin, C., Ducrocq, V., & Giordani, H. (2006). Sensitivity of torrential rain events to the sea surface temperature based on high-resolution numerical forecasts. *Journal of Geophysical Research Atmospheres*, *111*(12), 1–19. https://doi.org/10.1029/2005JD006541.

Li, L., Gochis, D. J., Sobolowski, S., & Mesquita, M. D. S. (2017). Evaluating the present annual water budget of a Himalayan headwater river basin using a high-resolution atmosphere-hydrology model. *Journal of Geophysical Research*, *122*(9), 4786–4807. https://doi.org/10.1002/2016JD026279.

Senatore, A., Mendicino, G., Gochis, D. J., Yu, W., Yates, D. N., & Kunstmann, H. (2015). Fully coupled atmosphere-hydrology simulations for the central Mediterranean: Impact of enhanced hydrological parameterization for short and long time scales. *Journal of Advances in Modeling Earth Systems*, *7*(4), 1693–1715. https://doi.org/10.1002/2015MS000510.

Yucel, I., & Onen, A. (2014). Evaluating a mesoscale atmosphere model and a satellite-based algorithm in estimating extreme rainfall events in northwestern Turkey. *Natural Hazards and Earth System Sciences*, 14(3), 611–624. https://doi.org/10.5194/nhess-14-611-2014

Yucel, I., Onen, A., Yilmaz, K. K., & Gochis, D. J. (2015). Calibration and evaluation of a flood forecasting system: Utility of numerical weather prediction model, data assimilation and satellite-based rainfall. *Journal of Hydrology*, 523, 49–66. https://doi.org/10.1016/j.jhydrol.2015.01.042.